Supporting Information

Lee et al. 10.1073/pnas.1113573108

SI Materials and Methods

Fly Stocks from the Bloomington Stock Center. The UAS-*MJD-78Q*, UAS-*MJD-27Q*, UAS-*p35*, UAS-*actin-GFP*, UAS-*Rac1*, UAS-*Rac1-V12*, UAS-*Spir-GFP*, UAS-*Cappuccino-GFP*, UAS-*Rho1-GFP*, UAS-*Enabled*, UAS-*Rac2*, UAS-*myr-PAK*, UAS-*HA-LIMK1*, UAS-*Cofilin*, UAS-*Rho-V20*, UAS-*HSP-A1L*, UAS-*Lamin-GFP*, UAS-*Red-Stinger*, and *D42*-Gal4 fly lines were obtained from the Bloomington Stock Center.

Specific Expression of Pathogenic PolyQ Proteins in da Neurons. Severity and penetrance of polyQ-induced dendrite phenotypes in da neurons could be affected by use of different gal4 drivers. Thus, for consistency of the results, we used in all our experiments isogenized *ppk*-gal4, *221*-gal4, and *109(2)80*-gal4 drivers to induce pathogenic polyQ protein expression in class IV, class I, and dorsal cluster da neurons, respectively. When pathogenic SCA3 or SCA1 protein expression was induced in dorsal cluster da neurons by *109(2)80*-gal4 driver, partial and variable range of reduction of spine formation was observed in ddaA class III da neurons. RU486-inducible gene-switch experiments were done as previously described (1).

For genetic interaction study using MJD-78Q^{weak} transgene, we generated a fly line carrying isogenized UAS-*MJD-78Q*^{weak}, *ppk*-gal4 driver, and UAS-*mCD8-GFP*. When we crossed this line to *w1118* wild-type fly, progenies showed dendrite phenotypes in ∼80% of ddaC class IV da neurons at 25 °C (Fig. S1).

Live Imaging of Dendrite Morphologies. Live imaging was carried out using a Leica SP5 confocal system. More than five animals of the same genotype were examined, and images of dendrites of da neurons (ddaC class IV da neurons or dorsal cluster da neurons) in abdominal segments A2–A6 were taken. In all images, anterior is to the left and dorsal is up. Images were taken 120 h AEL unless specified. Because expressing pathogenic polyQ proteins except for MJD-78Q^{weak} tends to reduce the signal intensity of dendritic markers (mCD8-GFP and mRFP) in da neurons, we used about 30% higher detector gain for imaging dendrites of da neurons expressing these transgenes.

Sholl Analysis of Dendritic Arbors of Class IV da Neurons. Concentric circles with 10-μm increments were drawn around the soma, and the number of dendritic branches that intersected each circle was counted. In neurons expressing MJD-27Q and MJD-78Q, the number of branches increased progressively from proximal to distal, and the largest number of dendrite branches was found between 200 and 300 μm from the cell body. The number of intersections (the complexity of dendritic trees) was markedly reduced by MJD-78Q expression. Dendrites of ddaC class IV da neurons were analyzed with the Neurolucida program.

Live Time-Lapse Imaging of Dendrite Dynamics. Live time-lapse imaging (Fig. S3) was carried out using a Leica SP5 confocal system. Images of dendrites of ddaC class IV da neurons in abdominal segments A2–A6 were taken, and the images of the same region were retaken after 30 min to determine dynamic changes. Early third instar larvae (96 h AEL) were examined.

Statistical Analysis. Student's unpaired *t* test (Microsoft Office Excel's TTEST) and Fisher's exact test (www.graphpad.com/quickcalcs/index.cfm) were used for statistical comparison.

Genetic Interaction Study. Only MJD-78Q^{weak} transgene was used for genetic interaction study, because expressing other pathogenic polyQ transgenes could reduce the expression level of coexpressed transgenes. Dendrite phenotypes were examined in more than five animals of the same genotype.

1. Rumpf S, Lee SB, Jan LY, Jan YN (2011) Neuronal remodeling and apoptosis require VCP-dependent degradation of the apoptosis inhibitor DIAP1. *Development* 138: 1153–1160.

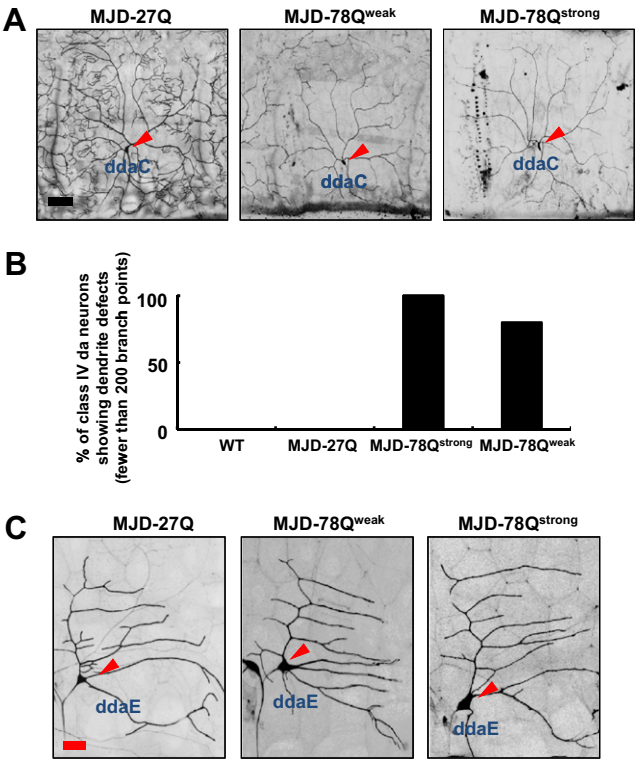

Fig. S1. Dendrite defects in class IV but not class I da neurons caused by weakly or strongly expressed MJD-78Q. (*A* and *C*) Images of dendrites of class IV (*A*) or I (*C*) da neurons expressing the denoted transgenes. Red arrowheads indicate cell bodies. (Scale bars: *A*, 100 μm; *C*, 30 μm.) (*B*) Quantitative analysis of the percent of class IV da neurons showing dendrite defects (n = 20).

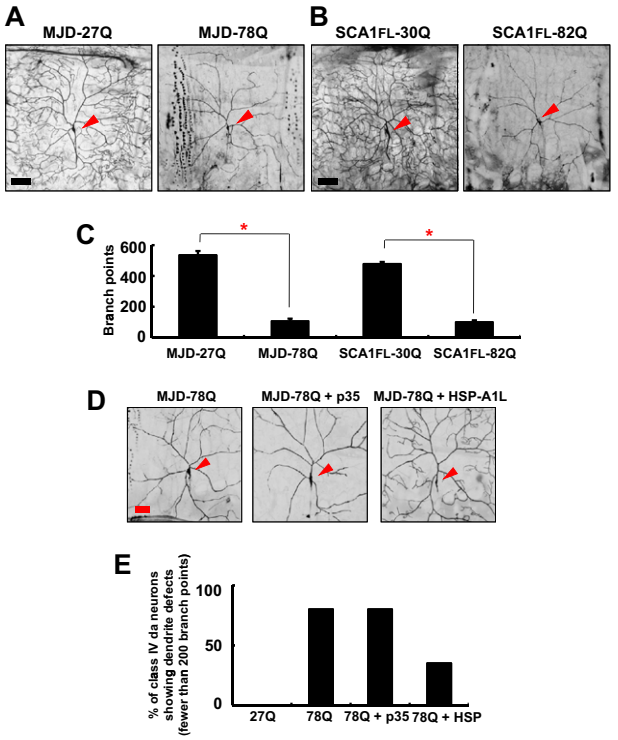

Fig. S2. PolyQ-induced dendrite defects were suppressed by chaperone proteins (HSP-A1L) but not p35. (*A*, *B*, and *D*) Images of dendrites of class IV da neurons expressing the denoted transgenes. Red arrowheads indicate cell bodies. (Scale bars: *A* and *B*, 100 μm; *D*, 50 μm.) (*C*) Quantitative analysis of the number of total dendrite branch points in ddaC class IV da neurons expressing the denoted transgenes. Bars indicate mean ± SD (n = 3). *P < 0.01 (Student's unpaired t test) relative to MJD-27Q or SCA1FL-30Q control. (*E*) Quantitative analysis of the percentage of class IV da neurons showing dendrite defects (n = 20).

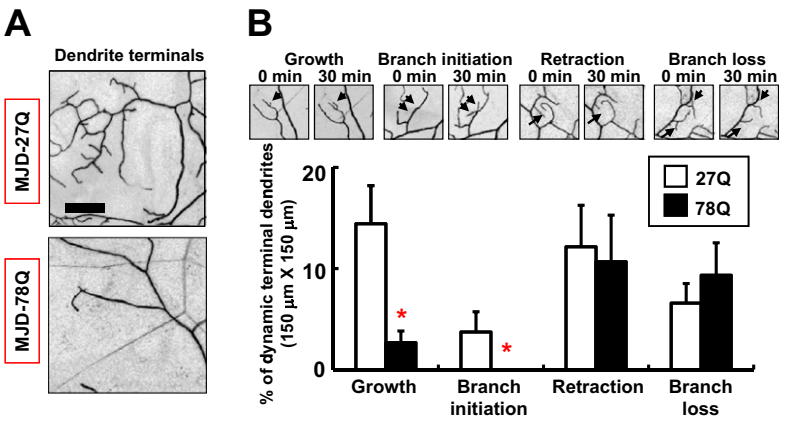

Fig. S3. PolyQ-induced defects in dendritic arbor formation mainly involve terminal branches. (*A*) Images showing terminal dendrites of class IV da neurons expressing the denoted transgenes. (Scale bar: 10 μm.) (*B*) PolyQ-induced defects in terminal dendrite growth in class IV da neurons. Representative dendritic changes in wild-type (*w1118*) class IV da neurons (*Upper*). PolyQ expression altered the percentage of dynamic terminal dendrites at 96 h AEL (*Lower*). Bars indicate mean ± SE ($n = 4$). *$P < 0.05$ (Student's unpaired *t* test) relative to MJD-27Q control.

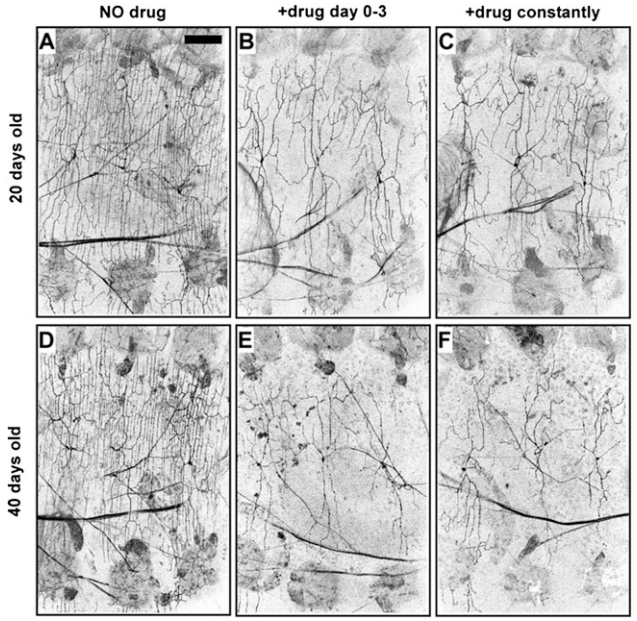

Fig. S4. PolyQ-induced dendrite phenotypes in adult da neurons are not efficiently reversed with aging after RU486 removal. (*A*–*F*) Dendrite images of adult da neurons from three adjacent abdominal segments. Flies were raised with different conditions of RU486 administration. Groups ($n = 3$) of flies were imaged 20 d (*A*–*C*) and 40 d (*D*–*F*) after eclosion. (Scale bar: 100 μm.)

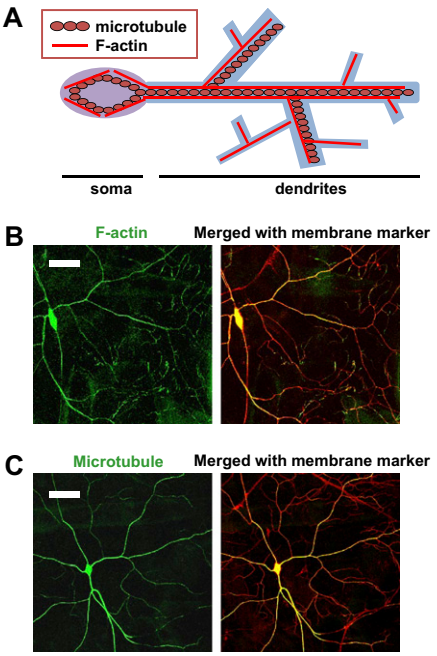

Fig. S5. Cytoskeletal structures in dendrites of class IV da neurons. (*A*) A schematic diagram showing F-actin and microtubular structures in dendrites of class IV da neurons. (*B* and *C*) F-actin (GMA; *B*) and microtubular (tau-GFP; *C*) structures in dendrites of class IV da neurons. *ppk*-gal4–driven expression of mRFP was used to mark dendrites of class IV da neurons (*Right*, red). (Scale bars: 30 μm.)

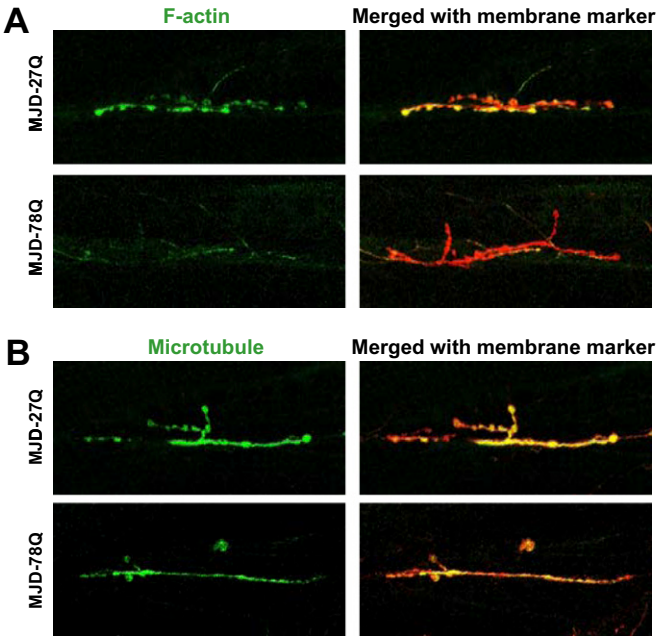

Fig. S6. PolyQ-induced F-actin defects in neuromuscular junction (NMJ). (*A*) F-actin structures (green) in NMJ of muscle 6/7 at segments A2–A5 visualized with *D42*-gal4–driven transgenic F-actin marker (GMA). *D42*-gal4–driven expression of mRFP was used to label NMJ (*Right*, red). Images were taken at 120 h AEL. (*B*) Microtubular structures (green) in NMJ of muscle 6/7 at segments A2–A5 visualized with *D42*-gal4–driven transgenic microtubule marker (tau-GFP). *D42*-gal4–driven expression of mRFP was used to label NMJ (*Right*, red). Images were taken at 120 h AEL.

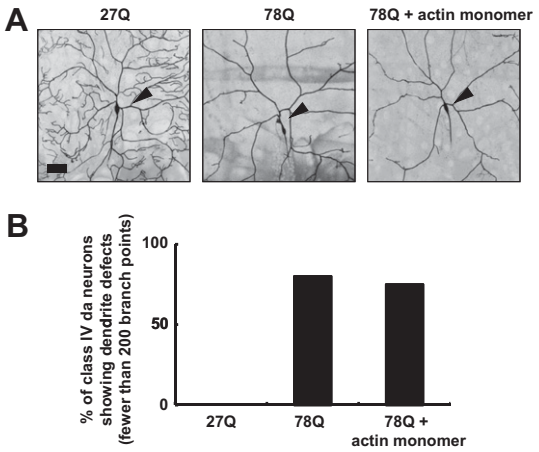

Fig. S7. Overexpression of actin monomers failed to mitigate polyQ-induced dendrite defects. (*A*) Images of dendrites of class IV da neurons expressing the denoted transgenes. Arrowheads indicate cell bodies. (Scale bar: 50 μm.) (*B*) Quantitative analysis of the percentage of class IV da neurons showing dendrite defects (n = 20).

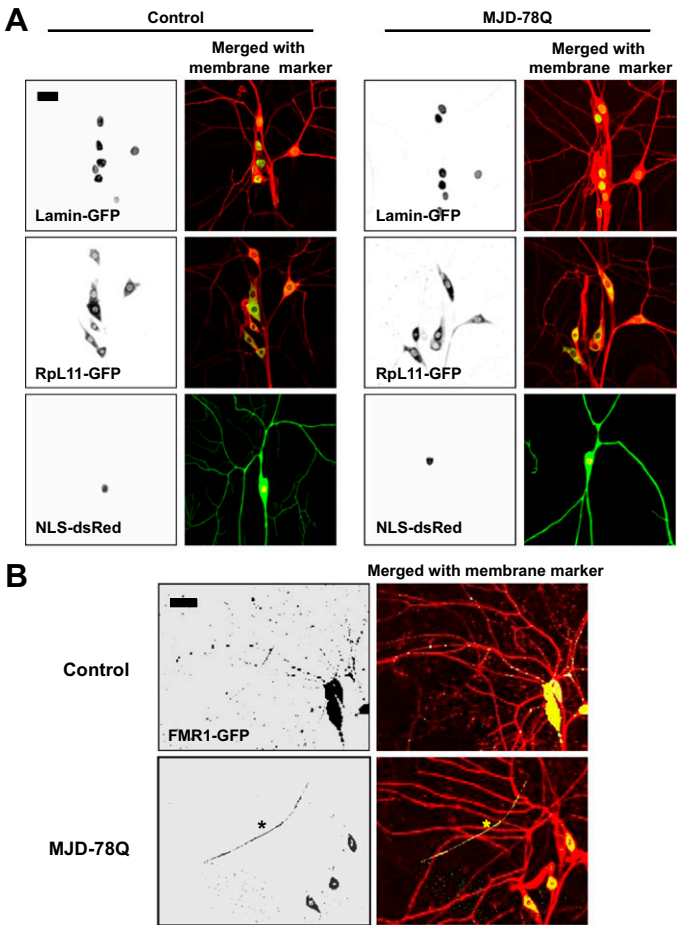

Fig. S8. Disrupted dendritic distribution of FMR1-positive granules in polyQ-expressing da neurons. (*A*) No obvious defects in the nuclear envelop structures, the subcellular distribution of ribosomal proteins undergoing nucleocytoplasmic shuttling, or the nuclear retention of nuclear-targeted proteins in polyQ-expressing da neurons. Images showing the nuclear envelop structures (Lamin-GFP), the subcellular distribution of ribosomal proteins (RpL11GFP), and the nuclear retention of nuclear-targeted proteins (Red Stinger, NLS-dsRed) in dorsal cluster da neurons or class IV da neurons expressing the denoted transgenes. (Scale bar: 30 μm.) (*B*) Images showing distribution of FMR1-positive granules (FMR1-GFP) in dorsal cluster da neurons expressing the denoted transgenes. Asterisks indicate an autofluorescent signal of the trachea. (Scale bar: 20 μm.)

Table S1. List of tested active forms of upstream regulators of actin regulatory machinery

Molecules	Terminal dendrite phenotype with MJD-78Q^{weak}	Percent of neurons showing modification of dendrite phenotypes
Rac1-V12	Strongly enhanced terminal branch formation	75
Myr-PAK	Partially enhanced terminal branch formation	40
Rho-V20	No effect	—

Table S2. List of tested wild-type forms of upstream regulators or components of actin regulatory machinery

Molecules	Terminal dendrite phenotype with MJD-78Q^{weak}	Percent of neurons showing modification of dendrite phenotypes
Upstream regulators		
Rac1	Enhanced terminal branch formation	60
Rac2	Enhanced terminal branch formation	55
Rho1	No effect	—
Actin regulators		
Profilin	No effect	—
Spir	No effect	—
Cappuccino	No effect	—
Enabled	No effect	—
LIMK1	No effect	—
Cofilin	No effect	—